The ligand-bound VDR, heterodimerized with retinoid X receptor (RXR), interacts with vitamin D response elements (VDREs) on regulatory regions of target genes, and recruits protein complexes that alter chromatin structure. They regulate expression of more than 900 vitamin D-responsive genes involved in calcium homeostasis, cell growth, differentiation, apoptosis, and modulation of immune response.[2] Importantly, the expression of the gene encoding MS-associated MHC class II allele HLA-DRB1*1501 is directly regulated by vitamin D via a VDRE on its promoter.[3]

A prospective case-control study on millions of US military personnel indicated that MS risk is decreased with increasing serum levels of 25-hydroxyvitamin D among white subjects.[4] Higher serum levels of 25-hydroxyvitamin D are associated with a greater suppressive capacity of regulatory T (Treg) cells in relapsing-remitting MS patients.[5] Calcitriol inhibits production of proinflammatory cytokines, such as IFNγ, IL-17, and IL-21, from human $CD4^+$ T cells, being responsible for the anti-inflammatory activity of vitamin D.[6] All of these observations support a protective role of vitamin D in immune cells against development of MS.[7] To elucidate underlying molecular mechanisms, it is important to characterize the global molecular network of VDR target genes (VDRTGs) presenting with diverse biological roles in immune cells, including those previously underestimated in immunopathogenesis of MS.

Recently, the rapid progress in the next-generation sequencing (NGS) technology has revolutionized the field of genome research. Notably, NGS thoroughly characterized the genetic basis of MS at the level of the whole genome of individual patients.[8] Chromatin immunoprecipitation followed by deep sequencing (ChIP-Seq) has been used as a NGS application to achieve genome-wide profiling of DNA-binding proteins, histone modifications, and nucleosomes.[9] ChIP-Seq with an advantage of higher resolution, less noise, and greater coverage of the genome, compared with the microarray-based ChIP-Chip method, and provides an innovative tool for studying the comprehensive gene regulatory networks. Since NGS analysis produces extremely high throughput experimental data, it is often difficult to extract the biologically meaningful implications. Recent advances in systems biology enable us to illustrate the cell-wide map of the complex molecular interactions by using the literature-based knowledgebase of molecular pathways.[10] The logically-arranged molecular networks construct the whole system, characterized by robustness, which maintains the proper function of the system in the face of genetic and environmental perturbations. Therefore, the integration of high-dimensional NGS data with underlying molecular networks serves as a rational approach to characterize the genome-wide network-based molecular mechanisms of gene regulation.

For an initial step to study molecular mechanisms underlying vitamin D-mediated protection against MS, we identified thousands of *in vivo* calcitriol-responsive VDRTG candidates collected from two public ChIP-Seq datasets of VDR-binding sites in human cells of B cell and monocyte origins, and investigated their molecular network by using three distinct pathway analysis tools of bioinformatics. We focused on the datasets derived from immune-relevant cell types of B cell and monocyte origins because B cells and monocytes play a key role in MS pathogenesis by serving as a source of proinflammatory and immunoregulatory cytokines and chemokines.[11]

Datasets and methods

Two distinct ChIP-Seq datasets of VDR-binding sites

We identified a comprehensive set of VDRTGs from two distinct ChIP-Seq datasets of VDR-binding sites numbered SRP002673 and SRP005910, retrieved from DDBJ Sequence Read Archive (DRA) (trace.ddbj.nig.ac.jp/DRASearch). SRP002673 contained the dataset of EBV-transformed human B lymphoblast cell lines (LCLs) isolated from two Centre d'Etude du Polymorphisme Humain (CEPH) individuals GM10855 and GM10861 who participated in the HapMap project.[12] The cells were treated with or without 100 nM calcitriol for 36 h, and then processed for ChIP-Seq using a rabbit anti-VDR antibody (sc-1008; Santa Cruz Biotechnology, USA). They were processed in parallel for transcriptome analysis on a Human Gene 1.0 ST Array (Affymetrix). We retrieved the transcriptome dataset numbered GSE22176 from Gene Expression Omnibus (GEO) (www.ncbi.nlm.nih.gov/gds). SRP005910 contained the dataset of THP-1 human monocyte leukemia cell line following exposure to 10 nM calcitriol or vehicle (ethanol) for 40 min for ChIP-Seq with a rabbit anti-VDR antibody (ab3508; Abcam) and for 4 h for transcriptome analysis on a Human-6 v2.0 Expression Beadchip (Illumina, San Diego, California, USA).[13] We retrieved the transcriptome dataset numbered GSE27270 from GEO. ChIP DNA fragments were processed for deep sequencing at a 35 bp (SRP002673) or a 36 bp (SRP005910) read length on the Genome Analyzer II (Illumina).

We mapped short reads of NGS data on the human genome reference sequence numbered hg19 by using Bowtie 0.12.7 (bowtie-bio.sourceforge.net). Then, we detected the statistically significant peaks of mapped reads by using Model-based Analysis of ChIP-Seq (MACS; liulab.dfci.harvard.edu/MACS) under the stringent condition of fold enrichment (FE)≥20 and the false discovery rate (FDR)≤1%. Finally, we identified genomic locations of the peaks by importing the processed data into GenomeJack v1.3, a novel genome viewer for NGS platforms (Mitsubishi Space Software; www.mss.co.jp/businessfield/bioinformatics). Based on RefSeq ID, the MACS peaks were categorized into those located on protein-coding genes with mRNA-

coding transcript (NM)-heading numbers, those on non-coding genes with non-coding transcript (NR)-heading numbers, and those located in intergenic regions without relevant neighboring genes. Since proximal promoters are generally located within several hundreds bp upstream of the transcription start site (TSS), the genomic locations of the summits were classified into the promoter region defined by the location within a 5 kb upstream from the 5' end of genes, the 5' untranslated region (5'UTR), the exon, the intron, and the 3'UTR. The locations outside these, which might include the locations of several distal promoters, were tentatively defined as intergenic regions, owing to the inability to accurately assess relevant target genes. The consensus motif sequences were identified by importing a 400 bp-length sequence surrounding the peak summit into MEME-ChIP (meme.sdsc.edu/meme/cgi-bin/meme-chip.cgi).

We also analyzed the transcriptome data of microarray analysis corresponding to the ChIP-Seq datasets. The log2-converted normalized data were evaluated by Welch's t-test to identify the genes differentially expressed between calcitriol-treated and control samples.

Molecular network analysis

To identify biologically relevant molecular networks and pathways, we imported Entrez Gene IDs of VDRTGs into the Functional Annotation tool of Database for Annotation, Visualization and Integrated Discovery (DAVID) v6.7 (david.abcc.ncifcrf.gov). DAVID identifies the most relevant pathway constructed by Kyoto Encyclopedia of Genes and Genomes (KEGG) (www.kegg.jp), composed of the genes enriched in the given set with an output of statistical significance evaluated by the modified Fisher's exact test. KEGG is a publicly accessible knowledgebase containing manually curated reference pathways that cover a wide range of metabolic, genetic and cellular processes, and human diseases, currently composed of 218,213 pathways generated from 435 reference pathways. We also imported Entrez Gene IDs into Ingenuity Pathways Analysis (IPA) (Ingenuity Systems; www.ingenuity.com) and KeyMolnet (Institute of Medicinal Molecular Design; www.immd.co.jp), both of which are commercial tools for molecular network analysis.

IPA is a knowledgebase that contains approximately 2,500,000 biological and chemical interactions and functional annotations with definite scientific evidence. By uploading the list of Gene IDs and expression values, the network-generation algorithm identifies focused genes integrated in a global molecular network. IPA calculates the score p-value, the statistical significance of association between the genes and the networks by the Fisher's exact test.

KeyMolnet contains knowledge-based contents on 150,500 relationships among human genes and proteins, small molecules, diseases, pathways and drugs.[10] They are categorized into the core contents collected from selected review articles with the highest reliability or the secondary contents extracted from abstracts of PubMed and Human Reference Protein database (HPRD). By importing the list of Gene IDs and expression values, the neighboring network-search algorithm selected one or more molecules as starting points to generate the network of all kinds of molecular interactions around starting molecules, including direct activation/inactivation, transcriptional activation/repression, and the complex formation within the designated number of paths from starting points. The generated network was compared side by side with 484 human canonical pathways of the KeyMolnet library. The algorithm counting the number of overlapping molecular relations between the extracted network and the canonical pathway makes it possible to identify the canonical pathway showing the most significant contribution to the extracted network.

Results

Identification of 2997 VDR target genes from two distinct ChIP-Seq datasets

By analyzing two distinct VDR-binding ChIP-Seq datasets numbered SRP002673 and SRP005910, derived from three samples of calcitriol-treated cells and three samples of non-treated or vehicle-treated (control) cells, we identified totally 4718 stringent ChIP-Seq peaks showing FE≥20 and FDR≤1% (Table 1). The genomic locations of the peaks were determined by using GenomeJack (Figure 1(a)). VDRE consensus sequences, comprising direct or inverted repeats of hexameric (G/A)G(G/T)TCA motifs with three intervening base pairs (DR3), were detected in the top 50 enriched genes in calcitriol-treated samples (Figure 1(b); Figure 2). After omitting the peaks located on non-coding genes and those located in intergenic regions, we identified 2997 peaks located on protein-coding genes that have their summits on the promoter (n=1353), 5'UTR (n=249), exon (n=85), intron (n=1253) or 3'UTR (n=57) (Table 1; Supplementary Tables 1–3 online). They are tentatively designated as ChIP-Seq-based VDRTGs.

Calcitriol-induced upregulation of a small set of ChIP-Seq-based VDR target genes

We also analyzed the transcriptome data numbered GSE22176 and GSE27270 corresponding to the ChIP-Seq datasets. Initially, we could not detect any genes differentially expressed between calcitriol-treated and control samples by the microarray-standard statistical evaluation with Welch's t-test followed by Bonferroni correction for multiple comparison, except for CD14 exhibiting a 6.65-fold increase in THP-1 cells by calcitriol treatment (p=0.0000004). Therefore, we attempted to extract greater numbers of calcitriol-responsive genes under the statistically less stringent condition of $p\leq0.05$ by Welch's t-test

Table 1. The overview of vitamin D receptor (VDR) target genes with stringent chromatin immunoprecipitation followed by deep sequencing (ChIP-Seq) peaks.

Datasets	Samples and treatment	Peaks on coding genes	Location of summits on coding genes					Peaks on non-coding genes	Peaks on intergenic regions	Total numbers of peaks
			Promoter	5'UTR	Exon	Intron	3'UTR			
SRP002673	**GM10855LCL-control**	54	39	8	1	5	1	8	6	68
	GM10855LCL-calcitriol	200	54	7	4	126	9	23	118	341
	GM10861LCL-control	402	281	63	7	48	3	41	70	513
	GM10861LCL-calcitriol	2047	875	161	50	919	42	223	1020	3290
SRP005910	**THP1-control**	108	55	5	14	34	0	15	63	186
	THP1-calcitriol	186	49	5	9	121	2	17	117	320
Total numbers of peaks		2997	1353	249	85	1253	57	327	1394	4718

By analyzing two distinct ChIP-Seq datasets of VDR-binding sites numbered SRP002673 and SRP005910, composed of three calcitriol-treated and three non-treated or vehicle-treated (control) samples, we identified stringent peaks exhibiting fold enrichment (FE)≥20 and false discovery rate (FDR)≤1%, which were categorized into the summits of the peaks located on protein-coding genes, those on non-coding genes and those in intergenic regions, by using GenomeJack.

without adjustment by Bonferroni correction and fold change ≥1.5 as upregulation or ≤0.75 as downreguation. This evaluation results in detection of overall 134 upregulated and 43 downregulated genes (Supplementary Tables 4–6 online). The set of 29 genes (21.6%) among 134 upregulated genes agreed with ChIP-Seq-based VDRTGs, including CLMN, PPP1R2, SPATA13, SULF2, P2RY8, MOBKL2B, CAMP, CD38, FAM116B, SERINC2, TRIM31, SLC25A20, TNFRSF17, ALDH1A1, CTSZ, ASAP2, SLC37A2, LRRC8A, TMEM37, C20orf197, PDZD7, SFXN3, PRKCH, SEMA4D, SEMA6B, CYTH4, ITGB5, ELF4, and ZMIZ1. In contrast, none of the downregulated genes have met with the list of ChIP-Seq-based VDRTGs.

Identification of 1541 ChIP-Seq-based calcitriol-responsive VDR target genes

Next, we combined all VDRTGs derived from three different calcitriol-treated samples into one, named the treatment set composed of 2432 genes, and those from three non-treated samples into one, named the non-treatment set composed of 564 genes. Thus, we found the constitutive binding of VDR on a genome-wide scale to a substantial number of genes in the absence of calcitriol treatment. Then, we extracted a non-redundant set of 1541 calcitriol-responsive genes that were detected exclusively in the treatment set (Supplementary Table 7 online).

Molecular network of 1541 calcitriol-responsive VDR target genes

By importing Entrez Gene IDs of 1541 calcitriol-responsive VDRTGs into the Functional Annotation tool of DAVID, we identified the top five most relevant KEGG pathways (Table 2). They include the pathways in cancer (hsa05200; p=4.92E–05), leukocyte transendothelial migration (hsa04670; p=1.17E–04) (Figure 3), systemic lupus erythematosus (hsa05322; p=5.57E–04), focal adhesion (hsa04510; p=7.30E–04), and Fcγ receptor-mediated phagocytosis (hsa04666; p=2.39E–03).

By using the Core Analysis tool of IPA, we identified the top five most relevant canonical pathways (Supplementary Table 8 online). They include Fcγ receptor-mediated phagocytosis in macrophages and monocytes (p=6.85E–07), molecular mechanisms of cancer (p=1.53E–06), macropinocytosis signaling (p=5.61E–06), glioma signaling (p=1.44E–05), and leukocyte extravasation signaling (p=2.03E–05). Thus, the results of KEGG and IPA showed a substantial overlap between the pathways constructed by VDRTGs, particularly whose function was involved in extravasation and phagocytosis of immune cells. IPA also extracted the top five most relevant functional networks. They include "Gene Expression, Protein Synthesis, Cellular Assembly and Organization" (p=1.00E–126), "Gene Expression, Cancer, Cardiovascular System Development and Function" (p=1.00E–116), "Cellular Function and Maintenance, Protein Degradation, Protein Synthesis" (p=1.00E–92), "Hematological System Development and Function, Tissue Morphology, Humoral Immune Response" (p=1.00E–88), and "Gene Expression, Cellular Development, Tissue Development" (p=1.00E–74) (Supplementary Table 9 online). Importantly, VDR serves as a hub molecule, on which the molecular connections are concentrated, in the functional network defined by "Gene Expression, Cellular Development, Tissue Development" (Figure 4).

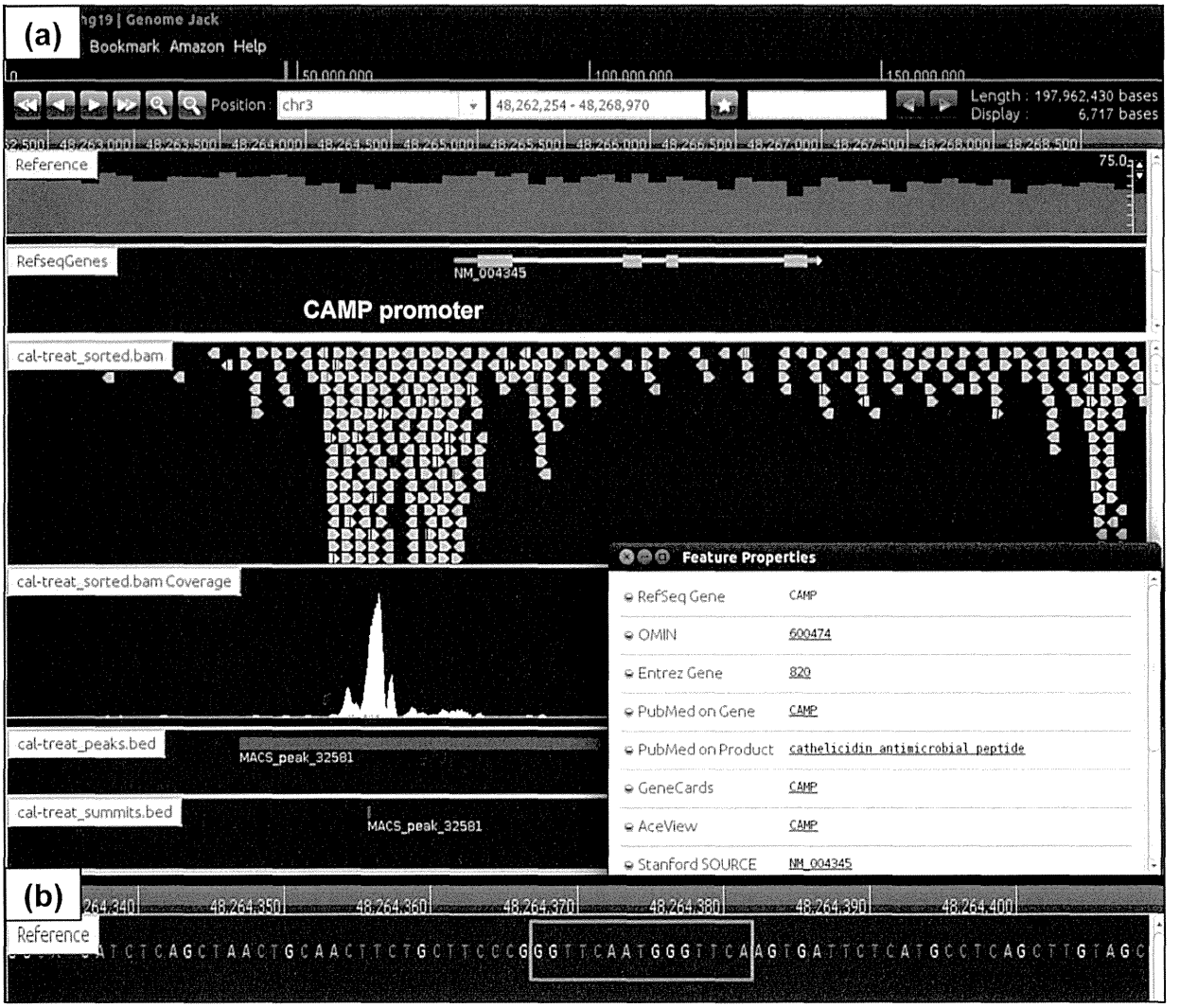

Figure 1. Identification of genomic locations of chromatin immunoprecipitation followed by deep sequencing (ChIP-Seq) peaks by GenomeJack.

By analyzing ChIP-Seq datasets of VDR-binding sites numbered SRP002673 and SRP005910, derived from 3 calcitriol-treated and 3 control samples, we identified totally 4718 peaks showing fold enrichment ≥ 20 and FDR ≤ 1% (Table 1). The genomic locations of the peaks were determined by importing the processed data into GenomeJack. An example of a vitamin D receptor (VDR) target gene named cathelicidin antimicrobial peptide (CAMP) (NM_004345) is shown, where a Model-based Analysis of ChIP-Seq (MACS) peak is located on the promoter region (a) with a vitamin D response element (VDRE) consensus sequence highlighted by orange (b). CAMP has been identified as a target gene for 1α,25-dihydroxyvitamin D3.[34]

By using KeyMolnet, the neighboring network search algorithm extracted a highly complex network, composed of 3300 molecules and 5569 molecular relations. The network exhibited a significant relationship with transcriptional regulation by retinoblastoma protein (Rb)/E2F family proteins (p=1.65E–182), transcriptional regulation by VDR (p=2.74E–171), transcriptional regulation by interferon regulatory factor (IRF) proteins (p=7.03E–103), heat shock protein 90 (HSP90) signaling pathway (p=9.33E–87), and histone acetyltransferase (HAT) signaling pathway (p=3.04E–79). Again, VDR plays a central role in homeostasis of the complex molecular network constructed by VDRTGs (Supplementary Figure 1 online).

Discussion

By using different antibodies, two distinct ChIP-Seq studies numbered SRP002673 and SRP005910 in human immune cells exposed to calcitriol identified 2776 and 2340 VDR-binding sites, respectively.[12,13] They utilized the similar mapping (Bowtie) and peak finding (MACS; FDR<1%) programs. Regardless of great variation of genetic and epigenetic regulation in distinct cell types,[14]

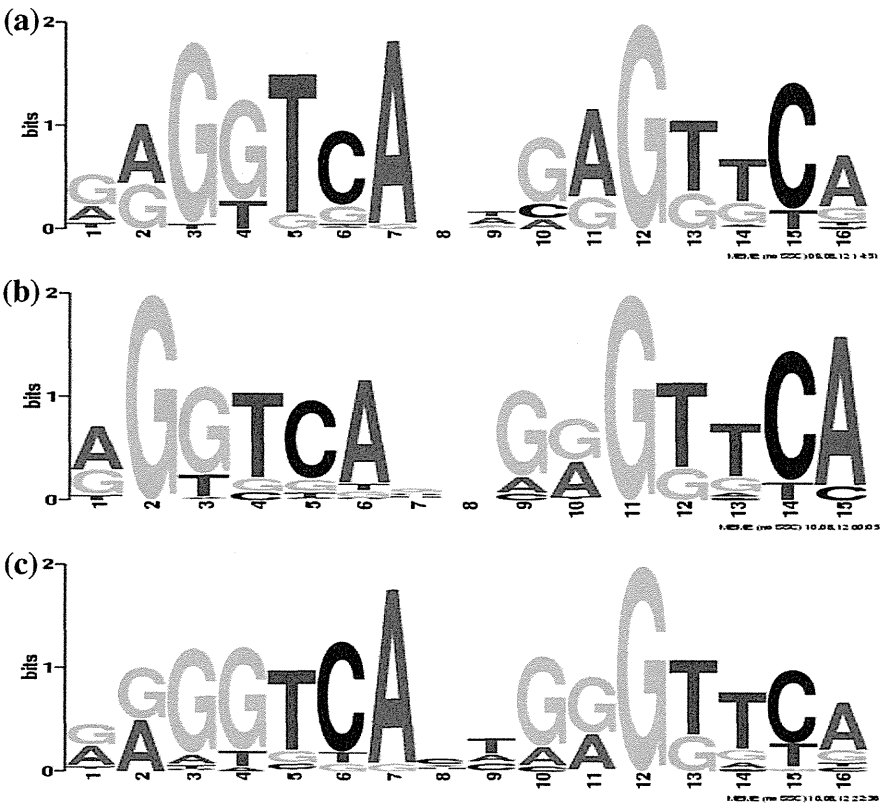

Figure 2. Motif analysis of vitamin D response element (VDRE) consensus sequences on chromatin immunoprecipitation followed by deep sequencing (ChIP-Seq) peaks. The consensus motif sequences were identified by importing a 400 bp-length sequence surrounding the summit of Model-based Analysis of ChIP-Seq (MACS) peaks of the top 50 enriched genes into the MEME-ChIP program. The direct repeats of hexameric (G/A)G(G/T)TCA motifs with three intervening base pairs (DR3) are found in calcitriol-treated samples of (a) GM10855, (b) GM10861, and (c) THP-1 cells.

Table 2. Top five Kyoto Encyclopedia of Genes and Genomes (KEGG) pathways relevant to 1541 calcitriol-responsive vitamin D receptor (VDR) target genes.

KEGG pathway	Molecules in pathway	*p*-value
hsa05200: pathways in cancer	ACVR1B, BCL2, BCL2L1, RUNX1, CDC42, CDK6, COL4A2, CRK, CTBP1, CTNNA1, CTNNB1, E2F2, MECOM, FGF14, GLI3, GRB2, GSK3B, HSP90AB1, ITGA3, LAMA3, LAMA5, LAMB3, LAMC1, MDM2, MSH3, NFKBIA, PDGFA, PLCG1, PLCG2, PRKCA, MAP2K1, PTCH1, PTEN, PTK2, RAC2, RAC3, RXRB, TCF7, TGFB1, HSP90B1, VEGFA, WNT8B, FGF17, TRAF4, PIK3R5, CTNNA3, WNT4, WNT10A, RASSF5, EGLN2	4.92E-05
hsa04670: leukocyte transendothelial migration	RHOH, CDC42, CTNNA1, CTNNB1, CYBA, GRLF1, ICAM1, ITGAL, ITGB2, CD99, NCF4, PLCG1, PLCG2, PRKCA, PTK2, RAC2, RAP1A, VAV1, VAV3, RAPGEF4, PIK3R5, CTNNA3, RASSF5, ESAM	1.17E-04
hsa05322: systemic lupus erythematosus	CD28, CD86, HIST1H2AE, HIST1H2AD, HIST1H2BD, HIST1H2BB, SNRPD3, HIST1H4I, HIST1H2AC, HIST2H2AA3, HIST2H2AC, HIST1H2BG, HIST1H2BL, HIST1H2BM, HIST1H2BF, HIST1H2BI, HIST1H2BO, HIST2H2BE, HIST1H3D, HIST1H4D, HIST1H4K, HIST1H4J, HIST1H4C, HIST1H4H, HIST1H4B, HIST1H4E, HIST2H4A, HIST1H2BJ, HIST1H2AH, HIST1H2BK, HIST2H3C, HIST2H3A, HIST2H2BF HIST2H2AA4	5.57E-04
hsa04510: focal adhesion	BCL2, CDC42, COL4A2, COL6A3, CRK, CTNNB1, GRB2, GRLF1, GSK3B, TNC, ITGA3, ITGB5, LAMA3, LAMA5, LAMB3, LAMC1, PDGFA, PPP1CA, PRKCA, MAP2K1, PTEN, PTK2, RAC2, RAC3, RAP1A, RASGRF1, SRC, VAV1, VEGFA, VAV3, PIK3R5, PDGFD	7.30E-04
hsa04666: Fc gamma R-mediated phagocytosis	CDC42, CRK, INPP5D, PLCG1, PLCG2, PRKCA, PRKCD, PRKCE, MAP2K1, RAC2, VAV1, PIP5K1B, PPAP2C, ASAP2, ARPC2, VAV3, PIK3R5, ARPC5L	2.39E-03

By importing Entrez Gene IDs of 1541 calcitriol-responsive VDR target genes into the Functional Annotation tool of Database for Annotation, Visualization and Integrated Discovery (DAVID), the top five most relevant KEGG pathways were identified. The *p*-value represents statistical significance evaluated by the modified Fisher's exact test.

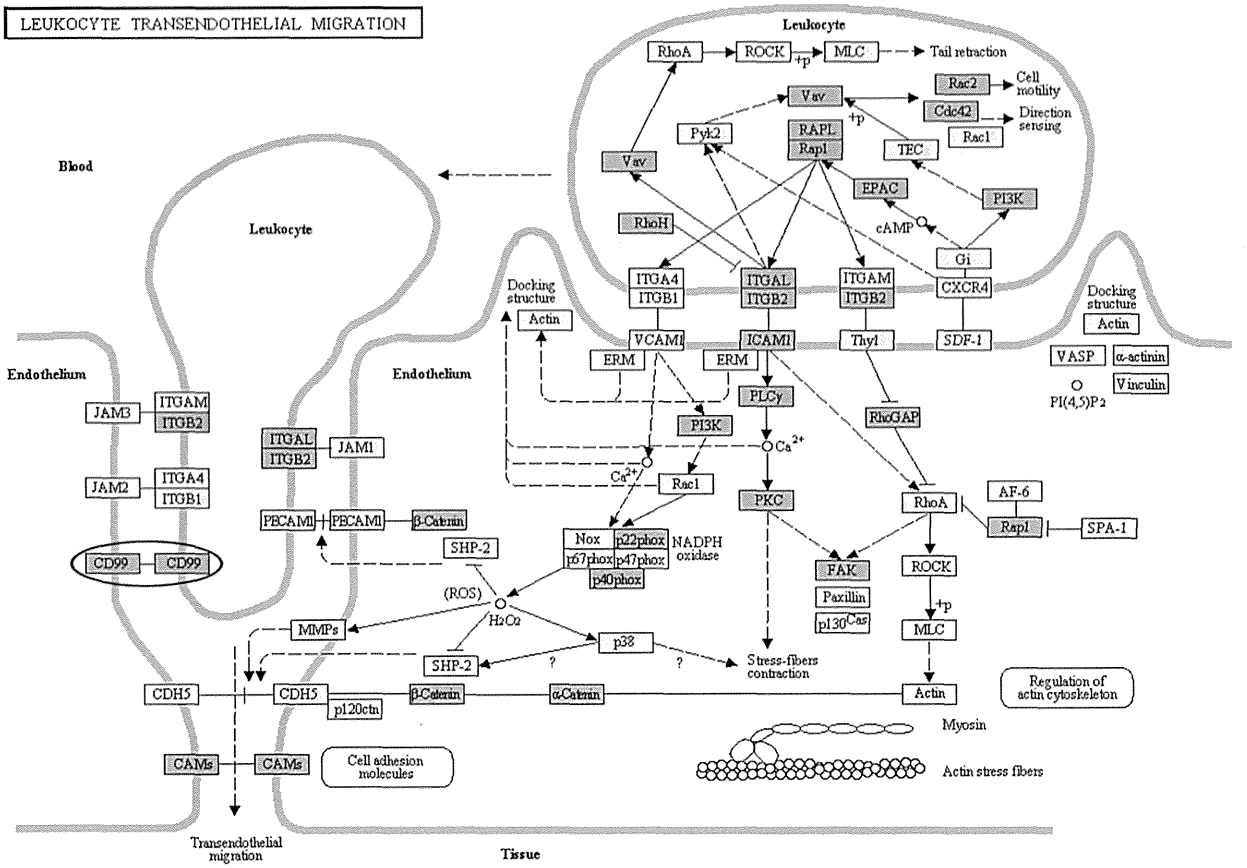

Figure 3. Molecular network of chromatin immunoprecipitation followed by deep sequencing (ChIP-Seq)-based vitamin D receptor (VDR) target genes by Kyoto Encyclopedia of Genes and Genomes (KEGG). The second rank relevant pathway defined by "leukocyte transendothelial migration (hsa04670)" is shown, where VDR target genes (VDRTGs) are colored by orange. CD99, a cell-surface glycoprotein involved in T cell migration and apoptosis, is encircled by a blue ellipse.

VDR-binding sites showed a considerable overlap (18.2%) between the cells originated from B cells and monocytes.[15] However, these studies did not clarify the global molecular network of genome-wide VDRTGs, with respect to immunomodulatory function of vitamin D potentially involved in protection against the development of MS. The ChIP-Seq analysis of VDR target genes derived from lymphocytes of MS patients appears to be preferable, if they are available. As an alternative, we reanalyzed the publicly available datasets of two immune-relevant cells, the cells of B cell and monocyte origins, and combined the results of both to retrieve *in vivo* VDRTG candidates as much as possible.

Although ChIP-Seq serves as a highly efficient method for genome-wide profiling of DNA-binding proteins, it requires some technical considerations:[16] the specificity of the antibody, reproducibility of the results, sequencing depth, and the source of controls, along with cell types, developmental stages, and culture conditions capable of affecting epigenetic features, constitute critical factors. In general, DNA-binding of transcription factors is a highly dynamic process. However, the ChIP-Seq data reflect a snapshot of binding actions. Motif analysis of a defined set of high-quality peaks makes it possible to evaluate the antibody specificity to some extent.[16] We identified VDRE consensus sequences around ChIP-Seq peak summits of all three calcitriol-treated samples, supporting the validity of the experiments. It is not unusual that some biologically important sites show fairly weak ChIP-Seq signals, whereas some sites with very high signals fail to give positive functional output in follow-up experiments.[16] We identified overall 2997 stringent ChIP-Seq peaks located on protein-coding genes. However, by transcriptome analysis, only 20% of upregulated genes and none of downregulated genes in calcitriol-treated cells agreed with ChIP-Seq-based VDRTGs. Most importantly, the molecular network of 1541 calcitriol-responsive VDRTGs is closely related to leukocyte transendothelial migration, Fcγ receptor-mediated phagocytosis, and transcriptional regulation by VDR, suggesting a pivotal role of VDRTGs in immune regulation.

The ligand-bound VDR, heterodimerized with RXR, interacts with VDRE sequences on regulatory regions of target genes.[2] VDR binding to VDREs is ligand-dependent,

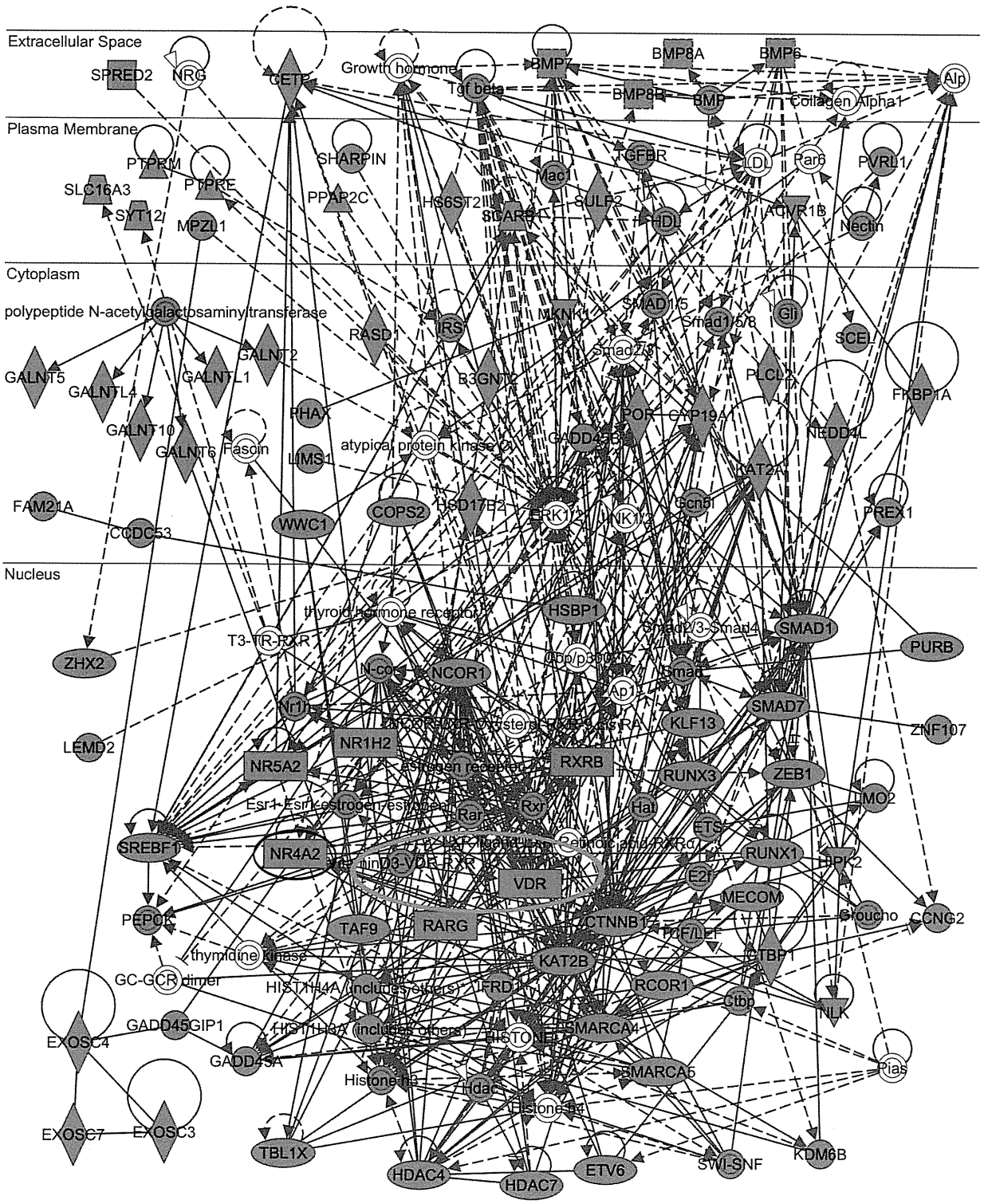

Figure 4. Molecular network of chromatin immunoprecipitation followed by deep sequencing (ChIP-Seq)-based vitamin D receptor (VDR) target genes by Ingenuity Pathways Analysis (IPA). By importing Entrez Gene IDs of the set of 1541 calcitriol-responsive VDR target genes (VDRTGs) into the Core Analysis tool of IPA, we identified the top five most relevant functional networks (Supplementary Table 9 online). The fifth rank relevant network defined by "Gene Expression, Cellular Development, Tissue Development" is shown, where VDRTGs are colored by red. VDR and VDR/ retinoid X receptor (RXR) complex are highlighted by an orange ellipse, while NR4A2, a nuclear orphan receptor involved in differentiation of Th1, Th17, and Treg cells, is encircled by a blue ellipse.

while RXR binding is ligand-independent.[17] VDREs are often multiple, composed of a pair of hexameric binding sites arranged as direct or inverted repeats interspaced by typically three (DR3) but a varying number of nucleotides different in the context of target genes.[18] We identified 2997 VDR-binding ChIP-Seq peaks distributed on protein-coding genes with location of the summits on the promoter (45.1%), 5'UTR (8.3%), exon (2.8%), intron (41.8%) or 3'UTR (1.9%). Thus, the peaks were concentrated in the promoter and intronic regions having VDRE motifs. The accumulation of VDREs in introns of VDR target genes is not unusual, because VDR-binding sites are located at a frequency of 44% within introns and exons but at only 13% in classical promoter regions in mouse preosteoblasts.[19] Furthermore, VDRE sequences are located occasionally in distant intergenic regions far from target gene promoters.[20] Upon binding to VDRE, the VDR-RXR heterodimer recruits protein complexes that alter the chromatin structure, either open for transcriptional activation or closed for transcriptional repression.[21] For transcriptional activation of target genes, the complex is comprised of CBP/p300 and SRC1 that exhibit histone acetyltransferase (HAT) activity, accompanied by accumulation of ATP-dependent chromatin remodeling complex. For transcriptional repression, the VDR-RXR heterodimer, capable of interfering with cognate transcription factors for expression of their target genes, recruits co-repressors, such as NCOR1, NCOR2, and COPS2, resulting in accumulation of histone deacetylases (HDAC) and DNA methyltransferases (DMT). However, by transcriptome analysis, we did not detect calcitriol-repressed genes having ChIP-Seq-based stringent VDR-binding sites. A recent study suggests that long-term binding is coupled to transcriptional activation, whereas fast binding and turnover is linked to lower levels of transcriptional output, indicating a pivotal role of transcriptional factor-binding dynamics across the genome for fine tuning of expression levels.[22]

The original ChIP-Seq studies of VDR-binding sites corresponding to the datasets we analyzed are quite different in the concentration and exposure time of calcitriol, i.e. B lymphoblast cell lines with 100 nM calcitriol for 36 h[12] versus THP-1 monocyte cell lines with 10 nM calcitriol for 40 min.[13] However, both studies consistently identified a DR3-type VDRE as major VDR-binding sites, although within 100 bp of ChIP-Seq peak summits, only less than 40% of the peaks actually contain DR3.[15] Importantly, one of these studies showed that genetic loci associated with MS susceptibility detected by genome-wide association study (GWAS) are enriched for VDR-binding sites accumulated in active regulatory regions of chromatin.[12,22] The other study found the most significant relevance of upregulated VDR target genes to the intracellular signaling cascade by using the gene ontology (GO) analysis with GeneTrail.[13]

We found that the complex molecular network of 1541 calcitriol-responsive VDRTGs is functionally related to leukocyte transendothelial migration and Fcγ receptor-mediated phagocytosis. These observations propose a scenario that vitamin D deficiency in MS patients could cause aberrant regulation of leukocyte and macrophage functions by disorganizing autoregulatory loops of the molecular network. Migration of activated T cells and monocytes into the brain across the disrupted blood-brain barrier (BBB) plays a key role in the development of active demyelinating lesions in MS. Vitamin D reduces the clinical severity of experimental autoimmune encephalomyelitis (EAE), an animal model of MS, by stimulating T cell apoptosis and inhibiting monocyte recruitment in the CNS.[24] We identified CD99, a cell-surface glycoprotein involved in T cell migration and apoptosis,[25] as one of calcitriol-responsive VDRTGs, potentially serving as a novel therapeutic target for MS (Figure 3). TCR signaling upregulates VDR expression on T cells, and subsequently elevates the levels of expression of PLCG1, a signaling molecule pivotal for T cell activation.[26] We also identified PLGC1 as a calcitriol-responsive VDRTG (Supplementary Table 7 online).

NR4A2, a member of the nuclear receptor superfamily, whose expression is greatly upregulated in T cells of active MS patients,[27] plays a key role in differentiation of Th1, Th17, and Treg cells with relevance to induction of autoimmunity. We identified NR4A2 as a calcitriol-responsive VDRTG (Figure 4). Transcription factors RUNX1 and RUNX3 are essential for induction and suppressive function of $Foxp3^+$ inducible Treg (iTreg) cells,[28] and both are calcitriol-responsive VDRTGs (Supplementary Table 7 online), suggesting a crucial role of vitamin D in immune tolerance induction. Furthermore, we identified EBI3, a component of anti-inflammatory cytokine IL-35 produced mainly by Treg cells,[29] as a calcitriol-responsive VDRTG (Supplementary Table 7 online).

B cells play an active role in the immunopathogenesis of MS.[30] They constitute lymphoid follicle-like structures ectopically located in the meninges of secondary progressive MS (SPMS) patients. We identified CXCR5, the receptor for the B-cell attractant CXCL13 produced by monocytes,[31] as a calcitriol-responsive VDRTG (Supplementary Table 7 online). Importantly, vitamin D itself regulates development and functionality of B cells.[30] Fcγ receptors act as a major phagocytotic receptor of macrophages/monocytes and microglia for ingestion of opsonized myelin. The expression of FCER1G is elevated in chronic MS lesions, and FCER1G-knockout mice show improved recovery from EAE.[32] Fcγ receptor-mediated phagocytosis requires cell membrane extension with cytoskeletal organization regulated by Rho family GTPase proteins, such as Rac1 and CDC42.[33] We identified CDC42 as one of calcitriol-responsive VDRTGs (Supplementary Table 7 online).

In conclusion, we found that the molecular network of 1541 calcitriol-responsive VDRTGs is linked to leukocyte transendothelial migration, Fcγ receptor-mediated phagocytosis, and transcriptional regulation by VDR.

These results suggest a pivotal role of genome-wide VDRTGs in immune regulation and tolerance induction. These observations propose the working hypothesis that persistent deficiency of vitamin D might perturb the complex network of VDRTGs in immune cells, being responsible for induction of an autoimmune response causative for MS. Further studies, including VDR ChIP-Seq analysis of purified populations of Th17, Th1, Treg, B cells, and monocytes derived from the serum vitamin D-sufficient and insufficient MS patients during relapse and remission, are required to evaluate this hypothesis.

Conflict of interest

The authors declare that they have no competing interests.

Funding

This work was supported by grants to J-IS from Research on Intractable Diseases (H21-Nanchi-Ippan-201 and H22-Nanchi-Ippan-136), the Ministry of Health, Labour and Welfare (MHLW), Japan, and the High-Tech Research Center Project (S0801043), the Grant-in-Aid (C22500322), the Ministry of Education, Culture, Sports, Science and Technology (MEXT), Japan.

References

1. Ascherio A, Munger KL and Simon KC. Vitamin D and multiple sclerosis. *Lancet Neurol* 2010; 9: 599–612.
2. Wang TT, Tavera-Mendoza LE, Laperriere D, et al. Large-scale in silico and microarray-based identification of direct 1,25-dihydroxyvitamin D3 target genes. *Mol Endocrinol* 2005; 19: 2685–2695.
3. Ramagopalan SV, Maugeri NJ, Handunnetthi L, et al. Expression of the multiple sclerosis-associated MHC class II Allele HLA-DRB1*1501 is regulated by vitamin D. *PLoS Genet* 2009; 5: e1000369.
4. Munger KL, Levin LI, Hollis BW, et al. Serum 25-hydroxyvitamin D levels and risk of multiple sclerosis. *JAMA* 2006; 296: 2832–2838.
5. Smolders J, Thewissen M, Peelen E, et al. Vitamin D status is positively correlated with regulatory T cell function in patients with multiple sclerosis. *PLoS One* 2009; 4: e6635.
6. Jeffery LE, Burke F, Mura M, et al. 1,25-Dihydroxyvitamin D3 and IL-2 combine to inhibit T cell production of inflammatory cytokines and promote development of regulatory T cells expressing CTLA-4 and FoxP3. *J Immunol* 2009; 183: 5458–5467.
7. Hanwell HE and Banwell B. Assessment of evidence for a protective role of vitamin D in multiple sclerosis. *Biochim Biophys Acta* 2011; 1812: 202–212.
8. Baranzini SE, Mudge J, van Velkinburgh JC, et al. Genome, epigenome and RNA sequences of monozygotic twins discordant for multiple sclerosis. *Nature* 2010; 464: 1351–1356.
9. Park PJ. ChIP-seq: Advantages and challenges of a maturing technology. *Nat Rev Genet* 2009; 10: 669–680.
10. Satoh JI, Tabunoki H and Yamamura T. Molecular network of the comprehensive multiple sclerosis brain-lesion proteome. *Mult Scler* 2009; 15: 531–541.
11. Romme Christensen J, Börnsen L, Hesse D, et al. Cellular sources of dysregulated cytokines in relapsing-remitting multiple sclerosis. *J Neuroinflammation* 2012; 9: 215.
12. Ramagopalan SV, Heger A, Berlanga AJ, et al. A ChIP-seq defined genome-wide map of vitamin D receptor binding: associations with disease and evolution. *Genome Res* 2010; 20: 1352–1360.
13. Heikkinen S, Väisänen S, Pehkonen P, et al. Nuclear hormone 1α,25-dihydroxyvitamin D3 elicits a genome-wide shift in the locations of VDR chromatin occupancy. *Nucleic Acids Res* 2011; 39: 9181–9193.
14. Fairfax BP, Makino S, Radhakrishnan J, et al. Genetics of gene expression in primary immune cells identifies cell type-specific master regulators and roles of HLA alleles. *Nat Genet* 2012; 44: 502–510.
15. Carlberg C, Seuter S and Heikkinen S. The first genome-wide view of vitamin D receptor locations and their mechanistic implications. *Anticancer Res* 2012; 32: 271–282.
16. Landt SG, Marinov GK, Kundaje A, et al. ChIP-seq guidelines and practices of the ENCODE and modENCODE consortia. *Genome Res* 2012; 22: 1813–1831.
17. Pike JW, Meyer MB, Martowicz ML, et al. Emerging regulatory paradigms for control of gene expression by 1,25-dihydroxyvitamin D3. *J Steroid Biochem Mol Biol* 2010; 121: 130–135.
18. Bouillon R, Carmeliet G, Verlinden L, et al. Vitamin D and human health: Lessons from vitamin D receptor null mice. *Endocr Rev* 2008; 29: 726–776.
19. Meyer MB, Goetsch PD and Pike JW. Genome-wide analysis of the VDR/RXR cistrome in osteoblast cells provides new mechanistic insight into the actions of the vitamin D hormone. *J Steroid Biochem Mol Biol* 2010; 121: 136–141.
20. Kim S, Yamazaki M, Zella LA, et al. Activation of receptor activator of NF-κB ligand gene expression by 1,25-dihydroxyvitamin D3 is mediated through multiple long-range enhancers. *Mol Cell Biol* 2006; 26: 6469–6486.
21. Fleet JC, DeSmet M, Johnson R, et al. Vitamin D and cancer: A review of molecular mechanisms. *Biochem J* 2012; 441: 61–76.
22. Lickwar CR, Mueller F, Hanlon SE, et al. Genome-wide protein-DNA binding dynamics suggest a molecular clutch for transcription factor function. *Nature* 2012; 484: 251–255.
23. Disanto G, Sandve GK, Berlanga-Taylor AJ, et al. Vitamin D receptor binding, chromatin states and association with multiple sclerosis. *Hum Mol Genet* 2012; 21: 3575–3586.
24. Pedersen LB, Nashold FE, Spach KM, et al. 1,25-dihydroxyvitamin D3 reverses experimental autoimmune encephalomyelitis by inhibiting chemokine synthesis and monocyte trafficking. *J Neurosci Res* 2007; 85: 2480–2490.
25. Manes TD and Pober JS. Identification of endothelial cell junctional proteins and lymphocyte receptors involved in transendothelial migration of human effector memory $CD4^+$ T cells. *J Immunol* 2011; 186: 1763–1768.
26. Von Essen MR, Kongsbak M, Schjerling P, et al. Vitamin D controls T cell antigen receptor signaling and activation of human T cells. *Nat Immunol* 2010; 11: 344–349.
27. Satoh J, Nakanishi M, Koike F, et al. Microarray analysis identifies an aberrant expression of apoptosis and DNA damage-regulatory genes in multiple sclerosis. *Neurobiol Dis* 2005; 18: 537–550.

28. Klunker S, Chong MM, Mantel PY, et al. Transcription factors RUNX1 and RUNX3 in the induction and suppressive function of Foxp3$^+$ inducible regulatory T cells. *J Exp Med* 2009; 206: 2701–2715.
29. Banchereau J, Pascual V and O'Garra A. From IL-2 to IL-37: The expanding spectrum of anti-inflammatory cytokines. *Nat Immunol* 2012; 13: 925–931.
30. Disanto G, Morahan JM, Barnett MH, et al. The evidence for a role of B cells in multiple sclerosis. *Neurology* 2012; 78: 823–832.
31. Krumbholz M, Theil D, Cepok S, et al. Chemokines in multiple sclerosis: CXCL12 and CXCL13 up-regulation is differentially linked to CNS immune cell recruitment. *Brain* 2006; 129: 200–211.
32. Lock C, Hermans G, Pedotti R, et al. Gene-microarray analysis of multiple sclerosis lesions yields new targets validated in autoimmune encephalomyelitis. *Nat Med* 2002; 8: 500–508.
33. Massol P, Montcourrier P, Guillemot JC, et al. Fc receptor-mediated phagocytosis requires CDC42 and Rac1. *EMBO J* 1998; 17: 6219–6229.
34. Wang TT, Nestel FP, Bourdeau V, et al. Cutting edge: 1,25-dihydroxyvitamin D3 is a direct inducer of antimicrobial peptide gene expression. *J Immunol* 2004; 173: 2909–2912.

Clinical & Experimental
Neuroimmunology

Clinical and Experimental Neuroimmunology 4 (2013) 19–28

ORIGINAL ARTICLE

Reactive astrocytes express the potassium channel Kir4.1 in active multiple sclerosis lesions

Jun-ichi Satoh,[1] Hiroko Tabunoki,[1] Tsuyoshi Ishida,[2] Yuko Saito,[3] Hidehiko Konno[4] and Kunimasa Arima[5]

[1]Department of Bioinformatics, Molecular Neuropathology, Meiji Pharmaceutical University, Tokyo, [2]Department of Pathology, Laboratory Medicine, Kohnodai Hospital, NCGM, Chiba, [3]Department of Laboratory Medicine, National Center Hospital, NCNP, Tokyo, [4]Department of Neurology, Nishitaga National Hospital, Sendai, [5]Department of Psychiatry, National Center Hospital, NCNP, Tokyo, Japan

Keywords
Alzheimer's disease; AQP4; Kir4.1; multiple sclerosis; reactive astrocytes

Correspondence
Jun-ichi Satoh, MD, Department of Bioinformatics and Molecular Neuropathology, Meiji Pharmaceutical University, 2-522-1 Noshio, Kiyose, Tokyo 204-8588, Japan.
Tel: +81-42-495-8678
Fax: +81-42-495-8678
Email: satoj@my-pharm.ac.jp

Received: 14 January 2013; revised: 18 February 2013; accepted: 19 February 2013.

Abstract

Objectives Kir4.1, an inwardly rectifying potassium channel expressed on perivascular and perisynaptic end-feet of astrocytes, plays a pivotal role in the spatial buffering of the potassium in the brain. A recent study showed that autoantibodies directed to Kir4.1 are detectable in the serum derived from approximately half of the patients with multiple sclerosis (MS) and clinically isolated syndrome, although their pathogenic roles should be elucidated.

Methods We studied Kir4.1 expression in MS and control brains by immunohistochemistry.

Results We found that reactive astrocytes expressed an intense immunoreactivity for Kir4.1 in active demyelinating lesions of MS, active lesion edges of neuromyelitis optica, ischemic lesion edges of cerebral infarction and neurodegenerative lesions of Alzheimer's disease. Reactive astrocytes accumulated in active MS lesions coexpressed Kir4.1 and AQP4. A subset of amyloid plaques in Alzheimer's disease brains also expressed Kir4.1. In contrast, infiltrating macrophages, activated microglia and surviving oligodendrocytes in active MS lesions did not express Kir4.1. Furthermore, cultured human astrocytes expressed Kir4.1, and the expression levels were not altered by exposure to tumor necrosis factor-α or interleukin-1β, but were elevated by transforming growth factor-β1.

Conclusions These results show that reactive astrocytes abundantly express Kir4.1, and Kir4.1 immunoreactivity is not lost in active demyelinating lesions of MS. (Clin. Exp. Neuroimmunol. doi: 10.1111/cen3.12011, March 2013)

Introduction

Kir4.1 is an adenosine triphosphate-dependent, inwardly rectifying potassium channel essential for the homeostasis of extracellular potassium, which forms a tetramer expressed on renal epithelial cells, inner ear cells, and perivascular and perisynaptic end-feet of astrocytes.[1,2] Kir4.1 is colocalized with the water channel, aquaporin-4 (AQP4), in the dystrophin-associated glycoprotein complex (DGC) at the interface of astrocytes and small blood vessels, where Kir4.1 cooperates with AQP4 for the spatial buffering of potassium and water transport.[3,4] Furthermore, the electrochemical gradient generated by K^+ buffering across the cell membrane of perisynaptic astrocytes regulates the uptake of extracellular glutamate.[5] Kir4.1 is expressed on cell bodies of oligodendrocytes in the rat optic nerve during development.[6] Kir4.1 knockout mice show motor impairment as a result of hypomyelination and axonal degeneration in the spinal cord, suggesting that Kir4.1 is indispensable for oligodendrocyte development.[7] The conditional knockout of astrocytic Kir4.1 leads to glial membrane depolarization, along with reduced clearance of the excitatory neurotransmitter glutamate, suggesting that Kir4.1 plays a key role in the regulation of neuronal excitability.[8] Supporting this view, loss of function mutations in the human KCNJ10 gene encoding Kir4.1 cause the epilepsy, ataxia, sensorineural deafness,

and tubulopathy (EAST)/seizure, sensorineural deafness, ataxia, mental retardation, and electrolyte imbalance (SeSAME) syndrome, characterized by epilepsy, ataxia, sensorineural deafness and renal tubulopathy.[9] Furthermore, the expression of Kir4.1, α-syntrophin and dystrophin is concurrently lost in perivascular end-feet of astrocytes in hippocampal sclerosis lesions of the patients with temporal lobe epilepsy.[10]

Accumulating evidence has indicated a pivotal role of B cells in the immunopathogenesis of multiple sclerosis (MS), an inflammatory demyelinating disease affecting mainly the human central nervous system (CNS) white matter.[11] More than 90% of MS patients show oligoclonal bands (OCB) in the cerebrospinal fluid (CSF), suggesting an intrathecal clonal expansion of B cells.[12] The meninges of MS patients often contain ectopic B cell follicles having germinal centers.[13] A subtype of acute demyelinating lesions of MS shows prominent deposition of immunoglobulins and complement activation.[14] Treatment with B cell-targeting monoclonal antibodies dramatically suppresses formation of new lesions in relapsing-remitting MS patients.[15]

A recent study showed that immunoglobulin G (IgG) autoantibodies directed to Kir4.1 are detectable in the serum derived from approximately half of the patients with MS, regardless of clinical subtypes, and clinically isolated syndrome (CIS), whereas they are barely detectable in the serum of the patients with other neurological diseases.[16] Intrathecal injection of serum anti-Kir4.1 IgG, in combination with human complement, reduced Kir4.1 expression on subpial and cortical astrocytes, accompanied by complement activation at antibody-binding sites in mouse brains *in vivo*.[16] However, the question remains to be clarified whether anti-Kir4.1 antibodies are pathogenic in the human brain. It is well known that anti-AQP4 antibodies are found in the serum derived from the great majority of patients with neuromyelitis optica (NMO), whereas they are rarely detectable in the serum of MS patients.[17] The active lesions of NMO show a profound loss of AQP4-expressing astrocytes.[18] Previously, we found that AQP4 expression is greatly enhanced in astrocytes and glial scars in active MS lesions.[19] Therefore, it is highly important to address the question whether or not Kir4.1 expression is lost in active demyelinating lesions of MS. The present study was designed to characterize Kir4.1 expression in active demyelinating lesions of MS by immunohistochemistry.

Methods

Human brain tissues

For immunohistochemistry, 10-μm thick serial sections of the cerebral cortex were prepared from

Table 1 Human brain tissues examined in the present study

Case no.	Age and sex	Clinical diagnosis	Cause of death
MS-1	29 Female	Secondary progressive multiple sclerosis	Asphyxia
MS-2	40 Female	Secondary progressive multiple sclerosis	Respiratory failure
MS-3	43 Female	Primary progressive multiple sclerosis	Hyperglycemia
MS-4	33 Male	Secondary progressive multiple sclerosis	Sepsis and multiple organ failure
NMO-1	70 Female	Devic's disease	Pneumonia
NC-1	88 Female	Neurologically normal subject	Myocardial infarction
NC-2	84 Male	Neurologically normal subject	Mmyocardial infarction
NC-3	77 Male	Neurologically normal subject	Lung cancer
NC-4	67 Male	Neurologically normal subject	Dissecting aortic aneurysm
CI-1	47 Male	Acute cerebral infarction	Sepsis
CI-2	84 Male	Acute cerebral infarction	Disseminated intravascular coagulation
CI-3	62 Male	Old cerebral infarction	Pancreatic cancer
CI-4	56 Male	Old cerebral infarction	Myocardial infarction
AD-1	59 Male	Alzheimer's disease	Pneumonia
AD-2	68 Female	Alzheimer's disease	Multiple organ failure
AD-3	80 Male	Alzheimer's disease	Pneumonia
AD-4	72 Male	Alzheimer's disease	Pneumonia
AD-5	77 Female	Alzheimer's disease	Pulmonary infarction

The present study includes four cases of multiple sclerosis (MS), one case of neuromyelitis optica (NMO), four cases of neurologically normal controls (NC), four cases of cerebral infarction (CI), and five cases of Alzheimer's disease (AD).

autopsied brains of four MS patients and 14 non-MS subjects (Table 1). All four MS cases were clinically diagnosed as chronic progressive MS.[20]

Non-MS cases included a previously reported case of neuromyelitis optica (NMO),[21] four neurologically normal control (NC) subjects, four patients with cerebral infarction (CI) and five patients with Alzheimer's disease (AD). All AD cases were satisfied with the Consortium to Establish a Registry for Alzheimer's Disease (CERAD) criteria for diagnosis of definite AD, and were categorized into the stage C of amyloid deposition and the stage VI of neurofibrillary degeneration, following the Braak staging system, as described previously.[22]

Autopsies were carried out at the National Center Hospital, National Center of Neurology and Psychiatry (NCNP), Kohnodai Hospital, National Center for Global Health and Medicine (NCGM), or the Nishitaga National Hospital. Comprehensive examination by four established neuropathologists (KA, YS, TI, HK) validated the pathological diagnosis. Written informed consent was obtained from all the cases. The Ethics Committee of the corresponding institutions approved the present study. The serum samples were not available from any of these cases.

Human astrocytes in culture

Cultured human astrocytes (AS) were established from primary cultures of neuronal progenitor (NP) cells isolated from human fetal brains (Cambrex, Walkersville, MD, USA), as described previously.[23] NP cell cultures were maintained in Dulbecco's modified Eagle's medium (DMEM)/F-12 medium (Invitrogen, Carlsbad, CA, USA) supplemented with an insulin-transferrin-selenium (ITS) supplement (Invitrogen), 20 ng/mL recombinant human epidermal growth factor (EGF) (Higeta, Tokyo, Japan), 20 ng/mL recombinant human basic fibroblast growth factor (bFGF) (PeproTech, London, UK) and 10 ng/mL recombinant human leukemia inhibitory factor (LIF) (Millipore, Temecula, CA, USA). For the induction of astrocyte differentiation, NP cells were incubated for several weeks in DMEM (Invitrogen) supplemented with 10% fetal bovine serum (FBS), 100 U/mL penicillin and 100 μg/mL streptomycin (feeding medium). The purity of astrocytes exceeded 98% by glial fibrillary acidic protein (GFAP) immunolabeling.[23] In some experiments, human astrocytes were incubated in the feeding medium supplemented with 50 ng/mL recombinant human transforming growth factor-β1 (TGF-β_1), tumor necrosis factor-α (TNF-α) or interleukin-1β (IL-1β) (all from PeproTech).

Immunohistochemistry and immunocytochemistry

After deparaffination, tissue sections were heated in 10 mmol/L citrate sodium buffer, pH 6.0 by autoclave at 110°C for 15 min in a temperature-controlled pressure chamber (Biocare Medical, Concord, CA, USA). They were treated at room temperature (RT) for 15 min with 3% hydrogen peroxide-containing methanol to block the endogenous peroxidase activity. The tissue sections were then incubated with phosphate-buffered saline (PBS) containing 10% normal goat serum at RT for 15 min to block non-specific staining. They were incubated in a moist chamber at 4°C overnight with a rabbit antibody against the C-terminal peptide of Kir4.1, whose sequence is conserved among the human, mouse and rat (1:2000; APC-035; Alomone Labs, Jerusalem, Israel), a rabbit antibody against the C-terminal peptide of human AQP4 (1:1000; sc-20812; Santa Cruz Biotechnology, Santa Cruz, CA, USA) or a rabbit anti-GFAP antibody (prediluted; N1506; Dako, Tokyo, Japan). After washing with PBS, the tissue sections were labeled at RT for 30 min with horseradish peroxidase (HRP)-conjugated secondary antibodies (Nichirei, Tokyo, Japan), followed by incubation with diaminobenzidine tetrahydrochloride (DAB) substrate (Vector, Burlingame, CA, USA). They were processed for a counterstain with hematoxylin. For negative controls, tissue sections were incubated with the Kir4.1 antibody (APC-035) preabsorbed with the specific peptide (Almone Labs). Non-astroglial cell types were identified by immunolabelling with cell type-specific antibodies.[24]

For double labeling, tissue sections and human astrocytes on glass slides were initially stained with a mixture of Kir4.1 antibody (APC-035) and a mouse monoclonal anti-GFAP antibody (GA5; Nichirei). They were then incubated with a mixture of Alexa Fluor 488-conjugated anti-rabbit IgG and Alexa Fluor 568-conjugated anti-mouse IgG (Invitrogen), followed by nuclear staining with 6'-diamidino-2-phenylindole (DAPI; Invitrogen). They were examined under the Olympus BX51 fluorescent microscope. Negative controls were processed following all the steps except for exposure to primary antibody.

Reverse transcription polymerase chain reaction analysis

DNase-treated total cellular RNA was processed for cDNA synthesis using oligo$(dT)_{12\text{-}18}$ primers and SuperScript II reverse transcriptase (Invitrogen). Then, cDNA was amplified by polymerase chain

reaction (PCR) using HotStar Taq DNA polymerase (Qiagen, Valencia, CA, USA), and a panel of sense and antisense primer sets following: 5'gttgtgaaagt ggcctctcctagt3' and 5'tcagacattgctgatgcgcacact3' for a 144 bp product of Kir4.1; 5'cctcgctggtggcctttatgagta3' and 5'gtctttccccttcttctcctctcc3' for a 218 bp product of AQP4; and 5'ccatgttcgtcatgggtgtgaacca3' and 5'gccagtagaggcagggatgatgttc3' for a 251 bp product of the glyceraldehyde-3-phosphate dehydrogenase (G3PDH) gene, serving as an internal control. The amplification program consisted of an initial denaturing step at 95°C for 15 min, followed by a denaturing step at 94°C for 1 min, an annealing step at 60°C for 40 s and an extension step at 72.9°C for 50 s for 35 cycles, except for G3PDH amplified for 28 cycles. For the positive control, total RNA of the human frontal cerebral cortex (Clontech, Mountain View, CA, USA) was processed in parallel for reverse transcription polymerase chain reaction (RT–PCR).

For quantitative RT–PCR (qPCR), cDNA was amplified by PCR in LightCycler ST300 (Roche Diagnostics, Tokyo, Japan) using SYBR Green I, and the set of sense and antisense primers described earlier. The expression levels of target genes were standardized against the levels of G3PDH detected in the corresponding cDNA samples. All the assays were carried out in triplicate.

Transient expression of Kir4.1 and AQP4 in HEK293 cells

Open reading frames (ORF) of the human KCNJ10 gene encoding Kir4.1 (GenBank NM_002241) and the human AQP4 gene (GenBank NM_001650) were amplified by PCR using PfuTurbo DNA polymerase (Stratagene, La Jolla, CA, USA), and sense and antisense primer sets following: 5'acgtcagttgccaaggtgtattac3' and 5'tcagacattgctgatgcgcacact3' for KCNJ10 and 5'agtgacagacccacagcaaggcgg3' and 5'tcatactgaagacaatacctctcc3' for AQP4. Then, they were cloned in an expression vector named pcDNA4/HisMax-TOPO (Invitrogen). Then, the vectors were transfected into HEK293 cells by using Lipofectamine 2000 reagent (Invitrogen). At 24 h after transfection, the cells were processed for western blot analysis.

Western blot analysis

To prepare total protein extract, the cells were homogenized in a non-denaturing lysis buffer composed of 20 mmol/L Tris-HCl, pH 8.0, 137 mmol/L NaCl, 1% Nonidet P40, 2 mmol/L ethylenediaminetetraacetic acid, and a cocktail of protease inhibitors, followed by centrifugation at 13200 g for 5 min at RT. The supernatant was separated on a 12% sodium dodecylsulfate-polyacrylamide gel electrophoresis gel. After gel electrophoresis, the protein was transferred onto nitrocellulose membranes, and immunolabeled at RT overnight with anti-Kir4.1 antibody (APC-035) or anti-AQP4 antibody (sc-20812). Then, the membranes were incubated at RT for 30 min with HRP-conjugated secondary antibodies (Santa Cruz Biotechnology). The specific reaction was visualized by using a chemiluminescent substrate (Pierce, Rockford, IL, USA). After the antibodies were stripped by incubating the membranes at 50°C for 30 min in a stripping buffer composed of 62.5 mmol/L Tris-HCl, pH 6.7, 2% sodium dodecylsulfate and 100 mmol/L 2-mercaptoethanol, the membranes were relabeled with a goat anti-heat shock protein HSP60 antibody (sc-1052; Santa Cruz Biotechnology), serving as an internal control for protein loading, or a mouse anti-Xpress antibody (R91025,; Invitrogen).

Results

Reactive astrocytes expressed Kir4.1 in chronic active demyelinating lesions of multiple sclerosis brains

First, to verify the specificity of anti-Kir4.1 antibody (APC-035), the ORF of either the human KCNJ10 gene or the human AQP4 gene cloned in the expression vector was expressed transiently as an Xpress-tagged protein in HEK293 cells. APC-035 reacted specifically with the recombinant Kir4.1 protein, but not with the AQP4 protein (Fig. 1a, lanes 1–3), whereas anti-AQP4 antibody (sc-20812) reacted with the recombinant AQP4 protein, but not with the Kir4.1 protein (Fig. 1b, lanes 1–3), validating the specificity of these antibodies.

Next, the expression of Kir4.1 was studied in brain tissue sections of four MS and 11 non-MS cases by immunohistochemistry using APC-035. In the brains of neurologically normal control (NC) subjects, an intense Kir4.1 immunoreactivity was identified chiefly in the vascular walls, in addition to the choroid plexus, the ependymal lining and the pial basement membrane (Fig. 2a). In NC brains, Kir4.1 immunoreactivity was almost absent in the capillaries, whereas vascular smooth muscle cells of larger vessels showed an intense immunoreactivity for Kir4.1.

In chronic active demyelinating lesions of MS, GFAP-positive reactive astrocytes expressed a very intense Kir4.1 immunoreactivity, whereas infiltrating myelin-phagocytosing macrophages, reactive microglia and surviving oligodendrocytes did not

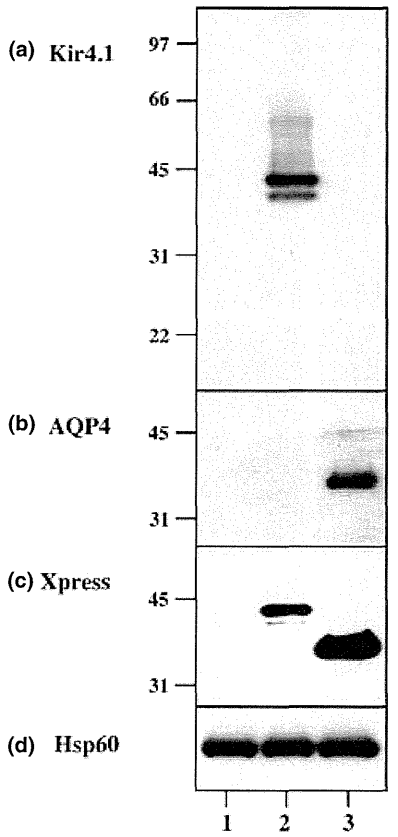

Figure 1 Validation of the specificity of anti-Kir4.1 antibody. The full-length protein of Kir4.1 or AQP4 fused with an Xpress tag was expressed in HEK293 cells, and the cellular protein extract was processed for western blot. (a) Kir4.1, (b) AQP4, (c) Xpress and (d) Hsp60, an internal control for protein loading. Lanes 1–3 indicate 15 μg of protein isolated from (1) non-transfected cells, (2) Kir4.1 expression vector-transfected cells and (3) AQP4 expression vector-transfected cells. The position of molecular weight size markers is shown on the left.

express Kir4.1 (Fig. 3a–e). Double labeling validated coexpression of Kir4.1 and GFAP in reactive astrocytes accumulated in active MS lesions (Fig. 4a–c). Reactive astrocytes in chronic active lesions of MS also coexpressed AQP4 (Fig. 3d–f). In contrast, in inactive MS lesions without accumulation of macrophages, Kir4.1 immunoreactivity on astrocytes was fairly weak or often absent. However, glial scar-forming astrocytes surrounding active demyelinating lesions and the glial scar were often intensely labeled with APC-035 (Fig. 3g). In contrast, Kir4.1 immunolabeling was totally absorbed by preincubation of APC-035 with the specific peptide (Fig. 3h). Notably, numerous hypertrophic reactive astrocytes accumulated in active lesion edges of NMO brains expressed an intense Kir4.1 immunoreactivity (Fig. 3i).

Reactive astrocytes expressed Kir4.1 in ischemic lesions and Alzheimer's disease brains

Reactive astrocytes accumulated in ischemic lesion edges, and the penumbra of acute and chronic cerebral infarction also expressed an intense Kir4.1 immunoreactivity, whereas foamy macrophages, reactive microglia and surviving oligodendrocytes did not express Kir4.1 (Fig. 2b,c). In neurodegenerative lesions of AD brains, reactive astrocytes, some neurons, the neuropil, the vascular walls and capillaries expressed Kir4.1 immunoreactivity at variable intensities (Fig. 2d–f). Notably, a subset (less than 5%) of amyloid plaques and perivascular deposits of amyloid were labeled with APC-035 (Fig. 2d,f).

Cultured human astrocytes constitutively expressed Kir4.1

Finally, we studied the expression of Kir4.1 in cultured human AS. By RT–PCR, we identified mRNA expression of Kir4.1 and AQP4 in both AS and NP cells, in addition to human brain tissues (Fig. 5a,b, lanes 1, 3 and 4). The levels of G3PDH, an internal control, were almost constant in the cells and tissues examined, whereas no products were amplified when the reverse transcription step was omitted (Fig. 5c, lanes 1–4). GFAP-immunoreactive AS intensely expressed Kir4.1 chiefly located on the cell surface by double-labeling immunocytochemistry (Fig. 4d–f). Next, we quantitatively studied Kir4.1 and AQP4 mRNA levels in AS after exposure to TNF-α, IL-1β or TGF-β1. The levels of expression of Kir4.1 and AQP4 were not altered in AS exposed to TNF-α or IL-1β (Fig. 5d,e) Although a trend for upregulation of Kir4.1 and downregulation of AQP4 was found in AS after exposure to TGF-β1, these alterations did not reach statistical significance. However, AS exposed to TGF-β1 showed a 1.49-fold increase in Kir4.1 protein levels by western blot, suggesting that TGF-β1 acts as a potential inducer of Kir4.1 expression in AS (Fig. 5f,g, lane 8).

Discussion

Kir4.1, an inward rectifying potassium channel expressed in renal epithelial cells, inner ear cells and glial cells in the CNS regulates the spatial buffering of extracellular potassium pivotal for glial function and neuronal excitability.[1,2,25] Recently, IgG autoantibodies directed to Kir4.1, binding to the first extracellular loop of Kir4.1, were detected in the serum derived from approximately half of MS and

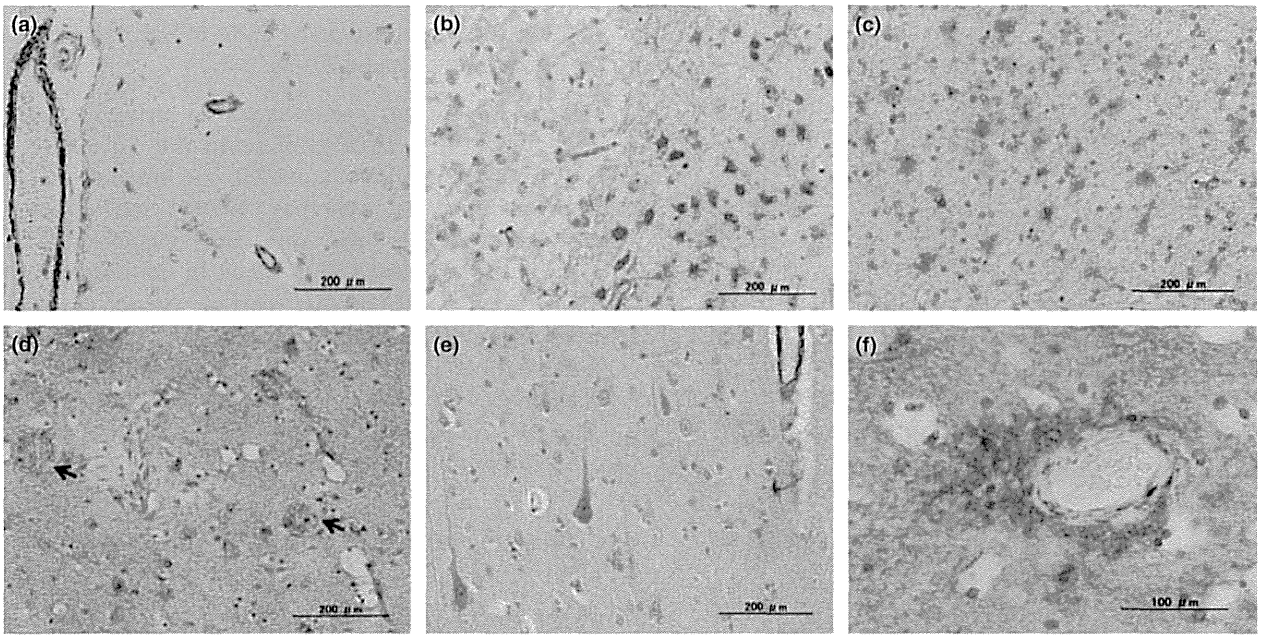

Figure 2 Kir4.1 expression in non-multiple sclerosis brains. The brain tissue sections of neurologically normal controls (NC), cerebral infarction (CI) and Alzheimer's disease (AD) were processed for immunohistochemistry with anti-Kir4.1 antibody. (a) NC, the temporal cortex, the vascular walls express Kir4.1. (b) Acute CI, the parietal cortex, Kir4.1-negative foamy macrophages on the left and Kir4.1-positive reactive astrocytes on the right. (c) Acute CI, the parietal white matter penumbra. (d) AD, the frontal cortex, Kir4.1-positive amyloid plaques (arrows). (e) AD, the frontal cortex, some neurons express Kir4.1. (f) AD, the frontal cortex, perivascular deposits of amyloid express Kir4.1.

CIS patients, although their pathogenic roles remain unknown.[16] The present study, by using immunohistochemistry, showed that reactive astrocytes express Kir4.1 in active demyelinating lesions of MS, active lesion edges of NMO, ischemic lesion edges of cerebral infarction and neurodegenerative lesions of AD. In contrast, infiltrating macrophages, activated microglia and surviving oligodendrocytes do not express Kir4.1. Thus, these observations show that Kir4.1 expression is not lost in active lesions of MS.

We found that cultured human AS express Kir4.1, and the levels of Kir4.1 on AS are not altered by exposure to pro-inflammatory cytokines, TNF-α and IL-1β, but upregulated modestly by TGF-β1, one of the gliosis-inducing cytokines.[26] In the mainstream of post-receptor signaling pathways, TGF-β1 utilizes SMAD proteins as a central signal transducer, whereas both TNF-α and IL-1β activate nuclear factor-κB (NF-κB), being responsible for the differential effects of these cytokines. In contrast to the present results, a recent study showed that IL-1β reduces Kir4.1 expression in cultured human AS isolated from a mixture of aborted fetal brains.[27] The apparent inconsistency is attributable to differences in cultured cells utilized. We found that reactive astrocytes accumulated in active MS lesions coexpress Kir4.1 and AQP4. A recent study showed that reactive astrocytes surviving in NMO brain lesions express AQP4 located on the cells surface and in cytoplasmic vesicles.[28]

Previous studies showed that Kir4.1 is expressed in both astrocytes and oligodendrocytes in the rat optic nerve,[6] and Kir4.1 knockout mice show an impaired ability to develop oligodendrocytes.[7] In contrast to the observations on rodent models, we did not identify Kir4.1 expression on oligodendrocytes existing in the white matter of MS and non-MS brains. This discrepancy is attributable to differences in the species, regions, and the stages of development and maturation. Supporting our observations, a previous study showed that Kir4.1 is expressed mainly in astrocytes surrounding synapses and blood vessels, but undetectable in the white matter in the adult rat brain.[1] In MS and non-MS brains, we identified Kir4.1 expression in vascular smooth muscle cells of larger vessels, in addition to vascular end-feet of astrocytes, being consistent with a recent study carried out on Kir4.1 expression in mouse mesenteric vascular smooth muscle cells.[29]

Increasing evidence indicates that Kir4.1 expression is regulated in a cell type-specific manner dependent on cellular growth and differentiation,

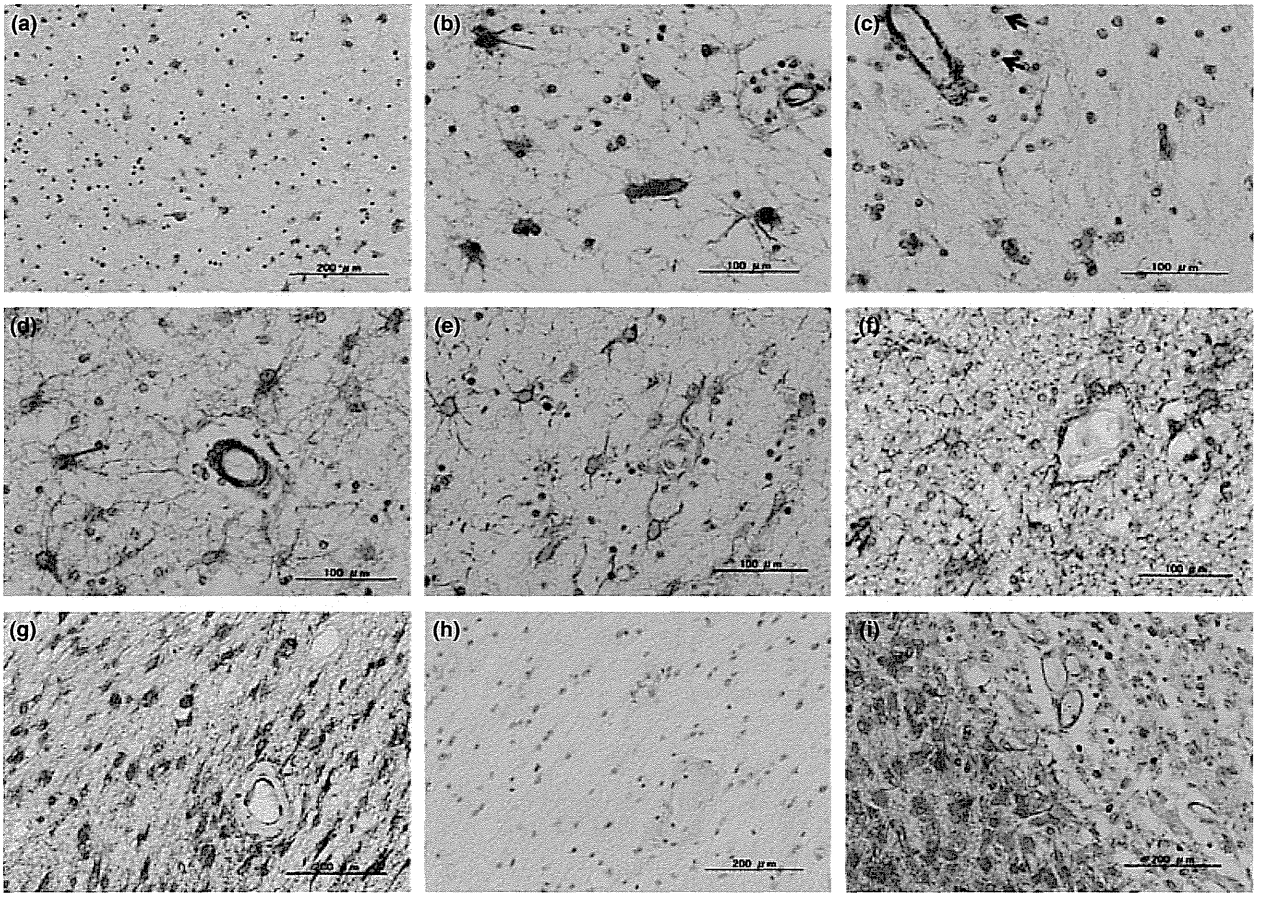

Figure 3 Kir4.1 expression in chronic active demyelinating lesions of multiple sclerosis (MS) brains. The brain tissue sections of MS and neuromyelitis optica (NMO) were processed for immunohistochemistry with anti-Kir4.1 antibody, anti-AQP4 antibody or anti-glial fibrillary acidic protein (GFAP) antibody. (a) Kir4.1, MS, the active demyelinating lesion center in the frontal white matter. (b) Kir4.1, the higher magnification of the same area as (a). (c) Kir4.1, MS, the active demyelinating lesion in the frontal white matter, perivascular foamy macrophages (arrows) do not express Kir4.1. (d) Kir4.1, MS, the frontal subcortical white matter. (e) GFAP, the same area as (d). (f) AQP4, the same area as (d), perivascular end-feet of reactive astrocytes express AQP4. (g) Kir4.1, MS, the periventricular white matter and glial scar-forming astrocytes express Kir4.1. (h) Kir4.1 absorbed by the specific peptide, the same area as (g). (i) Kir4.1, NMO, the active lesion edge in the frontal subcortical white matter and hypertrophic reactive astrocytes on the left express Kir4.1.

and in response to stress-inducing insults. A previous study showed that Kir4.1 channels are absent in immature, proliferating glial cells.[30] In these cells, upregulated expression of Kir4.1 correlates with astrocyte differentiation characterized by the establishment of a negative membrane potential and cell growth arrest. The levels of Kir4.1 expression are elevated in human astrocytic tumors with an increasing pathological grade.[31] Reactive gliosis induces redistribution of Kir4.1 in Müller cells from end-feet to cellular fibers, accompanied by inactivation of Kir4.1 channel function in a rabbit model of proliferative vitreoretinopathy.[32] Spinal cord injury causes a widespread loss of Kir4.1 and glutamate transporter 1 expression on astrocytes *in situ*.[33] Downregulation of Kir4.1 by RNAi in cultured rat astrocytes inhibits not only the potassium transfer, but also the glutamate uptake.[5] Progressive loss of Kir4.1 is identified in the spinal cord of the SOD1-G93A transgenic mouse model of amyotrophic lateral sclerosis (ALS), suggesting that higher extracellular concentrations of potassium and glutamate are responsible for induction of motor neuron cell death.[34]

We identified coexpression of Kir4.1 and AQP4 in reactive astrocytes in active MS lesions, supporting a functional interaction between Kir4.1 and AQP4 in the regulation of potassium and water transport.[3,4] A previous study showed that cerebral amyloid angiopathy (CAA) causes a loss of expression of both Kir4.1 and AQP4 from the astrocyte end-feet.[35] However, we found that some amyloid plaques and

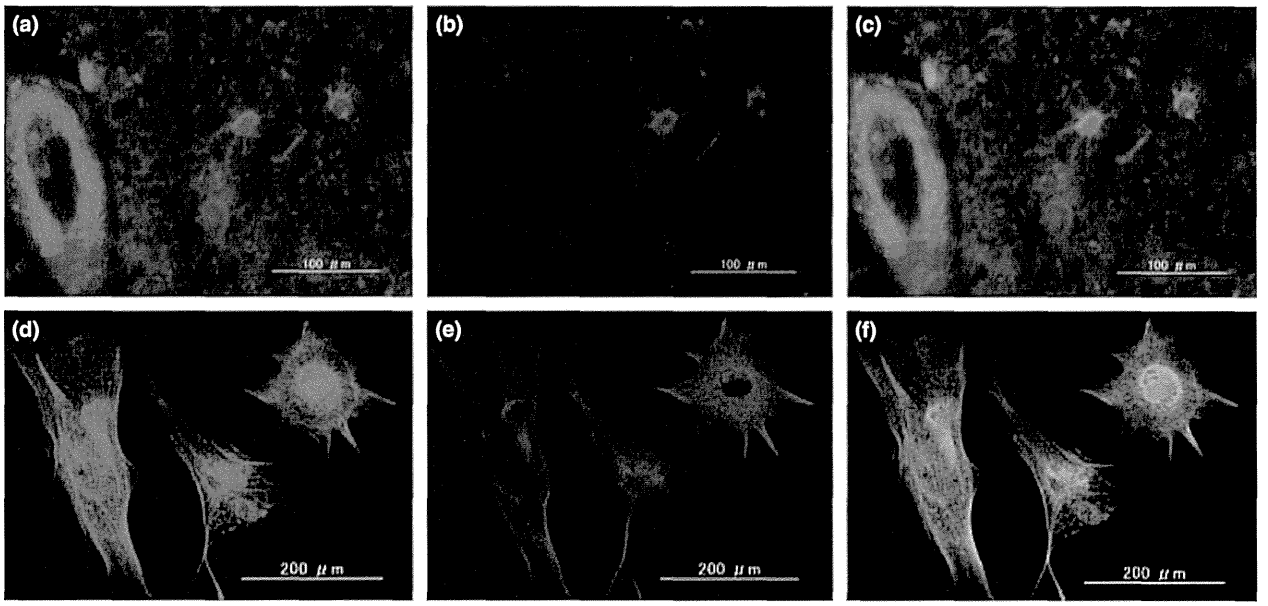

Figure 4 Coexpression of Kir4.1 and glial fibrillary acidic protein (GFAP). The (a–c) brain tissue section of active multiple sclerosis lesions and (d–f) cultured human astrocytes (AS) were processed for double labeling with anti-Kir4.1 antibody and anti-GFAP antibody. (a,d) Kir4.1, (b,e) GFAP and (c,f) merge with 6′-diamidino-2-phenylindole (DAPI) nuclear staining.

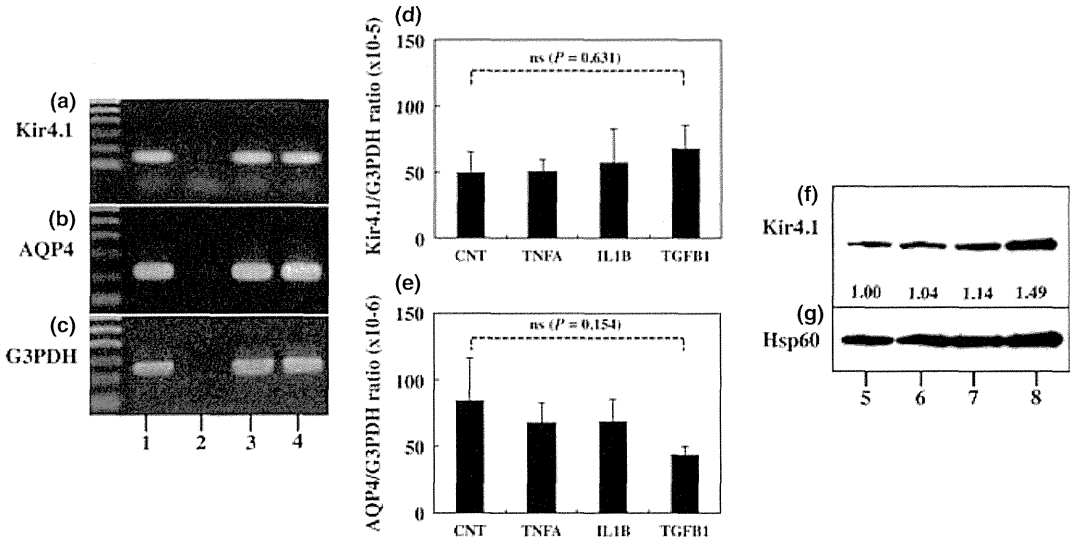

Figure 5 *Expression of Kir4.1 in cultured human astrocytes. cDNA prepared from cultured human astrocytes (AS) and neuronal progenitor (NP) cells* was processed for reverse transcription polymerase chain reaction (RT–PCR). (a) Kir4.1, (b) AQP4 and (c) G3PDH, an internal control. Lanes 1–4 indicate (1) the human frontal cerebral cortex (CBR) with inclusion of the reverse transcription (RT) step, (2) CBR omitting the RT step, (3) AS and (4) NP cells. AS exposed to 50 ng/mL tumor necrosis factor-α TNF-α, interleukin-1β (IL-1β) or transforming growth factor-β1 (TGF-β1), or untreated (CNT) were processed for quantitative RT–PCR (qPCR) and western blot. (d) Kir4.1 and (e) AQP4 expression on qPCR in AS after a 24-h exposure. No statistically significant differences (ns) are found among the treatments by one-way ANOVA with post-hoc Turkey's test. (f) Kir4.1 and (g) Hsp60 expression on western blot of 15 μg of protein isolated from AS after a 48-h exposure. Kir4.1 expression levels normalized by Hsp60 levels, an internal control for protein loading, are indicated in the panel (f). Lanes 5–8 indicate AS (5) untreated or exposed to (6) TNF-α, (7) IL-1β or (8) TGF-β1.

perivascular amyloid deposits moderately express Kir4.1. Importantly, Kir4.1 prevents swelling of astroglial processes in experimental spinal cord edema caused by hypotonic osmotic stress, suggesting a protective role of Kir4.1 expressed on astrocyte end-feet against aberrant water transport.[36]

At present, the precise mechanisms remain unknown as to how MS patients generate autoantibodies against KiR4.1, and how these antibodies induce pathogenic effects on demyelinated axons through defective transport of potassium, glutamate and water. Because astrocyte damage, called astrocytopathy, occurs not only in NMO lesions, but also in a subtype of active MS lesions,[37] we could put forward a possible scenario that Kir4.1-expressing reactive astrocytes damaged in active and aggressive MS lesions serve as a continuous source of immunogens, leading to sensitization of autoreactive lymphocytes in MS.

Acknowledgements

All autopsied brain samples were obtained from the Research Resource Network (RRN), Japan. This work was supported by grants to J-IS from Research on Intractable Diseases (H21-Nanchi-Ippan-201 and H22-Nanchi-Ippan-136), the Ministry of Health, Labour and Welfare (MHLW), Japan, and the High-Tech Research Center (HRC) Project (S0801043) and the Genome Research Center (GRC) Project and a Grant-in-Aid (C22500322), the Ministry of Education, Culture, Sports, Science and Technology (MEXT), Japan.

References

1. Higashi K, Fujita A, Inanobe A, Tanemoto M, Doi K, Kubo T, et al. An inwardly rectifying K^+ channel, Kir4.1, expressed in astrocytes surrounds synapses and blood vessels in brain. *Am J Physiol Cell Physiol.* 2001; **281**: C922–31.
2. Olsen ML, Sontheimer H. Functional implications for Kir4.1 channels in glial biology: from K^+ buffering to cell differentiation. *J Neurochem.* 2008; **107**: 589–601.
3. Guadagno E, Moukhles H. Laminin-induced aggregation of the inwardly rectifying potassium channel, Kir4.1, and the water-permeable channel, AQP4, via a dystroglycan-containing complex in astrocytes. *Glia.* 2004; **47**: 138–49.
4. Nagelhus EA, Mathiisen TM, Ottersen OP. Aquaporin-4 in the central nervous system: cellular and subcellular distribution and coexpression with KIR4.1. *Neuroscience.* 2004; **129**: 905–13.
5. Kucheryavykh YV, Kucheryavykh LY, Nichols CG, Maldonado HM, Baksi K, Reichenbach A, et al. Downregulation of Kir4.1 inward rectifying potassium channel subunits by RNAi impairs potassium transfer and glutamate uptake by cultured cortical astrocytes. *Glia.* 2007; **55**: 274–81.
6. Kalsi AS, Greenwood K, Wilkin G, Butt AM. Kir4.1 expression by astrocytes and oligodendrocytes in CNS white matter: a developmental study in the rat optic nerve. *J Anat.* 2004; **204**: 475–85.
7. Neusch C, Rozengurt N, Jacobs RE, Lester HA, Kofuji P. Kir4.1 potassium channel subunit is crucial for oligodendrocyte development and in vivo myelination. *J Neurosci.* 2001; **21**: 5429–38.
8. Djukic B, Casper KB, Philpot BD, Chin LS, McCarthy KD. Conditional knock-out of Kir4.1 leads to glial membrane depolarization, inhibition of potassium and glutamate uptake, and enhanced short-term synaptic potentiation. *J Neurosci.* 2007; **27**: 11354–65.
9. Scholl UI, Choi M, Liu T, Ramaekers VT, Häusler MG, Grimmer J, et al. Seizures, sensorineural deafness, ataxia, mental retardation, and electrolyte imbalance (SeSAME syndrome) caused by mutations in KCNJ10. *Proc Natl Acad Sci USA.* 2009; **106**: 5842–7.
10. Heuser K, Eid T, Lauritzen F, Thoren AE, Vindedal GF, Taubøll E, et al. Loss of perivascular Kir4.1 potassium channels in the sclerotic hippocampus of patients with mesial temporal lobe epilepsy. *J Neuropathol Exp Neurol.* 2012; **71**: 814–25.
11. Krumbholz M, Derfuss T, Hohlfeld R, Meinl E. B cells and antibodies in multiple sclerosis pathogenesis and therapy. *Nat Rev Neurol.* 2012; **8**: 613–23.
12. Owens GP, Bennett JL, Lassmann H, O'Connor KC, Ritchie AM, Shearer A, et al. Antibodies produced by clonally expanded plasma cells in multiple sclerosis cerebrospinal fluid. *Ann Neurol.* 2009; **65**: 639–49.
13. Serafini B, Rosicarelli B, Magliozzi R, Stigliano E, Aloisi F. Detection of ectopic B-cell follicles with germinal centers in the meninges of patients with secondary progressive multiple sclerosis. *Brain Pathol.* 2004; **14**: 164–74.
14. Lucchinetti C, Brück W, Parisi J, Scheithauer B, Rodriguez M, Lassmann H. Heterogeneity of multiple sclerosis lesions: implications for the pathogenesis of demyelination. *Ann Neurol.* 2000; **47**: 707–17.
15. Hauser SL, Waubant E, Arnold DL, Vollmer T, Antel J, Fox RJ, et al. B-cell depletion with rituximab in relapsing-remitting multiple sclerosis. *N Engl J Med.* 2008; **358**: 676–88.
16. Srivastava R, Aslam M, Kalluri SR, Schirmer L, Buck D, Tackenberg B, et al. Potassium channel KIR4.1 as an immune target in multiple sclerosis. *N Engl J Med.* 2012; **367**: 115–23.
17. Lennon VA, Wingerchuk DM, Kryzer TJ, Pittock SJ, Lucchinetti CF, Fujihara K, et al. A serum autoantibody marker of neuromyelitis optica: distinction from multiple sclerosis. *Lancet.* 2004; **364**: 2106–12.
18. Misu T, Fujihara K, Kakita A, Konno H, Nakamura M, Watanabe S, et al. Loss of aquaporin 4 in lesions of neuromyelitis optica: distinction from multiple sclerosis. *Brain.* 2007; **130**: 1224–34.

19. Satoh J, Tabunoki H, Yamamura T, Arima K, Konno H. Human astrocytes express aquaporin-1 and aquaporin-4 in vitro and in vivo. *Neuropathology*. 2007; **27**: 245–56.
20. Satoh J, Onoue H, Arima K, Yamamura T. Nogo-A and nogo receptor expression in demyelinating lesions of multiple sclerosis. *J Neuropathol Exp Neurol*. 2005; **64**: 129–38.
21. Satoh J, Obayashi S, Misawa T, Tabunoki H, Yamamura T, Arima K, et al. Neuromyelitis optica/Devic's disease: gene expression profiling of brain lesions. *Neuropathology*. 2008; **28**: 561–76.
22. Satoh J, Tabunoki H, Ishida T, Saito Y, Arima K. Immunohistochemical characterization of γ-secretase activating protein expression in Alzheimer's disease brains. *Neuropathol Appl Neurobiol*. 2012; **38**: 132–41.
23. Obayashi S, Tabunoki H, Kim SU, Satoh J. Gene expression profiling of human neural progenitor cells following the serum-induced astrocyte differentiation. *Cell Mol Neurobiol*. 2009; **29**: 423–38.
24. Satoh J, Tabunoki H, Ishida T, Yagishita S, Jinnai K, Futamura N, et al. Immunohistochemical characterization of microglia in Nasu-Hakola disease brains. *Neuropathology*. 2011; **31**: 363–75.
25. Bay V, Butt AM. Relationship between glial potassium regulation and axon excitability: a role for glial Kir4.1 channels. *Glia*. 2012; **60**: 651–60.
26. Moon LD, Fawcett JW. Reduction in CNS scar formation without concomitant increase in axon regeneration following treatment of adult rat brain with a combination of antibodies to TGFβ$_1$ and β$_2$. *Eur J Neurosci*. 2001; **14**: 1667–77.
27. Zurolo E, de Groot M, Iyer A, Anink J, van Vliet EA, Heimans JJ, et al. Regulation of Kir4.1 expression in astrocytes and astrocytic tumors: a role for interleukin-1β. *J Neuroinflammation*. 2012; **9**: 280.
28. Hinson SR, Romero MF, Popescu BF, Lucchinetti CF, Fryer JP, Wolburg H, et al. Molecular outcomes of neuromyelitis optica (NMO)-IgG binding to aquaporin-4 in astrocytes. *Proc Natl Acad Sci USA*. 2012; **109**: 1245–50.
29. Tajada S, Cidad P, Moreno-Domínguez A, Pérez-García MT, López-López JR. High blood pressure associates with the remodelling of inward rectifier K^+ channels in mice mesenteric vascular smooth muscle cells. *J Physiol*. 2012; **590**: 6075–91.
30. Higashimori H, Sontheimer H. Role of Kir4.1 channels in growth control of glia. *Glia*. 2007; **55**: 1668–79.
31. Tan G, Sun SQ, Yuan DL. Expression of Kir 4.1 in human astrocytic tumors: correlation with pathologic grade. *Biochem Biophys Res Commun*. 2008; **367**: 743–7.
32. Ulbricht E, Pannicke T, Hollborn M, Raap M, Goczalik I, Iandiev I, et al. Proliferative gliosis causes mislocation and inactivation of inwardly rectifying K^+ (Kir) channels in rabbit retinal glial cells. *Exp Eye Res*. 2008; **86**: 305–13.
33. Olsen ML, Campbell SC, McFerrin MB, Floyd CL, Sontheimer H. Spinal cord injury causes a wide-spread, persistent loss of Kir4.1 and glutamate transporter 1: benefit of 17 β-oestradiol treatment. *Brain*. 2010; **133**: 1013–25.
34. Kaiser M, Maletzki I, Hülsmann S, Holtmann B, Schulz-Schaeffer W, Kirchhoff F, et al. Progressive loss of a glial potassium channel (KCNJ10) in the spinal cord of the SOD1 (G93A) transgenic mouse model of amyotrophic lateral sclerosis. *J Neurochem*. 2006; **99**: 900–12.
35. Wilcock DM, Vitek MP, Colton CA. Vascular amyloid alters astrocytic water and potassium channels in mouse models and humans with Alzheimer's disease. *Neuroscience*. 2009; **159**: 1055–69.
36. Dibaj P, Kaiser M, Hirrlinger J, Kirchhoff F, Neusch C. Kir4.1 channels regulate swelling of astroglial processes in experimental spinal cord edema. *J Neurochem*. 2007; **103**: 2620–8.
37. Sharma R, Fischer MT, Bauer J, Felts PA, Smith KJ, Misu T, et al. Inflammation induced by innate immunity in the central nervous system leads to primary astrocyte dysfunction followed by demyelination. *Acta Neuropathol*. 2010; **120**: 223–36.